MULTIPLE SPACECRAFT OBSERVATIONS OF INTERPLANETARY SHOCKS: CHARACTERISTICS OF THE UPSTREAM ULF TURBULENCE

C.T. Russell
Institute of Geophysics and Planetary Physics
University of California
Los Angeles, California 90024

E.J. Smith and B.T. Tsurutani
Jet Propulsion Laboratory
Pasadena, California 91109

J.T. Gosling and S.J. Bame
Los Alamos National Laboratory
Los Alamos, New Mexico 87545

ABSTRACT

All interplanetary shocks observed by ISEE-3 and either ISEE-1 or ISEE-2 or both in 1978 and 1979 are examined for evidence of upstream waves. In order to characterize the properties of these shocks it is necessary to determine accurate shock normals. We invert an overdetermined set of equations to obtain shock normals, velocities and error estimates for all these shocks. Tests of the method indicate it is quite reliable. Using these normals we then calculate the Mach number and angle between the interplanetary magnetic field and the shock normal for each shock. These parameters allow us to separate the upstream waves into two classes: whistler-mode precursors which occur at low Mach numbers and upstream turbulence whose amplitude at Mach numbers greater than 1.5 is controlled by the angle of the field to the shock normal. The former waves are right-hand circularly polarized and quite monochromatic. The latter waves are more linearly polarized and have a broadband featureless spectrum.

Introduction

Upstream from the earth's bow shock there is a wide variety of wave phenomena, both at ULF and VLF frequencies (cf. Russell and Hoppe, 1983 and references therein). Similar wave phenomena are observed upstream from the bow shocks of Mercury, Venus and Jupiter (Hoppe and Russell, 1981). Interplanetary shocks differ from planetary bow shocks in that they have much larger radii of curvature and in general are weaker than planetary bow shocks. Thus it is of interest to compare the properties of waves upstream from interplanetary shocks with those upstream from planetary bow shocks. One such comparison has been made by Kennel et al. (1982) who showed that ion-acoustic-like waves occurred at VLF frequencies in front of interplanetary shocks, in a manner similar to the occurrence in front of the terrestrial bow shock. This observation suggests that there are upstream particle phenomena associated with interplanetary shocks. In fact, energetic particles are observed in front of some of these shocks (Gosling et al., 1983). Thus, we might expect to observe ULF wave phenomena there also.

We expect differences in the nature of these waves from those observed upstream of planetary bow shocks because of the different geometry of planetary bow shocks and their lower Mach numbers. For example, because the radius of curvature of the interplanetary shock is much greater than that of a planetary shock, the

time of connection of a field line to the shock is generally much greater for the interplanetary shock. Depending on how far upstream the shock associated energetic particles propagate, these waves may grow over a large region in front of the shock. In planetary bow shocks, in general, the waves grow in a very limited region defined by the field lines tangent to the nose of the bow shock, behind which any waves generated are convected downstream toward the bow shock by the solar wind.

Understanding these waves is important to further our knowledge of cosmic ray acceleration. One of the mysteries of cosmic rays is that they seem to be accelerated very efficiently. It is often suggested that cosmic ray acceleration is associated with interstellar shock waves produced by supernova explosions (e.g., Axford, 1981). Long after the explosion when the shock has expanded to large distances and is weak, the interstellar shock may resemble typical interplanetary shocks. It is important to note that cosmic rays are thought to be accelerated in a multi-step process with repeated scattering centers being necessary. The ULF waves, seen upstream of planetary bow shocks, are excellent candidates for these scattering centers if they indeed occur in front of interplanetary shocks. To date few studies of upstream turbulence have been undertaken. Morfill and Scholer (1977) examined power spectra of the interplanetary magnetic field in the period range 100 to 1000 seconds upstream and downstream of four interplanetary shocks. They found that the ULF power increased across these shocks but since the field strength increased a similar amount there was little change in the diffusion coefficient. They did not attempt to determine shock normal directions nor to relate wave properties to shock parameters. Russell and Hoppe (1983) in a preliminary study of these same shocks have shown that upstream wave turbulence is correlated with the angle between the upstream magnetic field and the shock normal. Most recently Tsurutani et al. (1983) have used minimum variance analysis to characterize the properties of waves seen upstream of interplanetary shocks.

In this paper, we examine the properties of the upstream turbulence and relate these properties to the parameters of the interplanetary shocks. To accomplish this we will use plasma and magnetic field data from the ISEE-1, -2 and -3 spacecraft. The plasma instrumentation has been described by Bame et al. (1978 a, b). The ISEE-1 magnetometer has been described by Russell (1978) and the ISEE -3 magnetometer by Frandsen et al. (1978). A difficult aspect of studying interplanetary shocks and the most critical, is determining their normals. Thus, before examining the properties of the waves we discuss the procedure we have used to obtain the best fit normals for these shocks.

Shock Normal Determination

Eighteen interplanetary shocks in the ISEE-1 and -2 records from 1978-1979 were selected for this study. Most of these were selected because of the simultaneous availability of ISEE-3 data. IMP-8 or Prognoz 7 measurements were also available for some of these shocks. Five of the shocks were observed by four spacecraft. Under such conditions it is possible to determine the average shock orientation from the time delays and separation vectors between the spacecraft. This has been done for these five shocks and the analysis reported elsewhere (Russell et al., 1983a, b).

As a result of these analyses we have developed the following technique for determining the shock normal, $\underline{N}$, using an over-determined set of equations.

First, the separation vectors and separation times are used:

$$\begin{pmatrix} \underline{\Delta x}_{10} \\ \underline{\Delta x}_{20} \\ \vdots \end{pmatrix} \cdot \begin{pmatrix} Nx \\ Ny \\ Nz \end{pmatrix} = V \begin{pmatrix} \Delta t_{10} \\ \Delta t_{20} \\ \vdots \end{pmatrix}$$

where $\underline{\Delta x}_{i0}$ and Δt_{i0} are the separation vectors and time lags between satellite 'i' and satellite '0'. Then the change in vector magnetic field $\underline{\Delta B}_1$ is incorporated:

$$\begin{pmatrix} \underline{\Delta B}_0 \\ \underline{\Delta B}_1 \\ \vdots \end{pmatrix} \cdot \begin{pmatrix} Nx \\ Ny \\ Nz \end{pmatrix} = 0$$

Velocity coplanarity is also used when 3-D plasma data are available on both sides of the shock.

$$\begin{pmatrix} (\underline{B}_u \times \underline{\Delta V})_0 \\ (\underline{B}_u \times \underline{\Delta V})_1 \\ \vdots \end{pmatrix} \cdot \begin{pmatrix} Nx \\ Ny \\ Nz \end{pmatrix} = 0$$

and

$$\begin{pmatrix} (\underline{B}_d \times \underline{\Delta V})_0 \\ (\underline{B}_d \times \underline{\Delta V})_1 \\ \vdots \end{pmatrix} \cdot \begin{pmatrix} Nx \\ Ny \\ Nz \end{pmatrix} = 0$$

where $\underline{B}_u$ and $\underline{B}_d$ are the upstream and downstream fields and $\underline{\Delta V}$ is the change in the velocity across the shock. Magnetic coplanarity can also be used whenever the upstream and downstream fields are separated by a sufficiently large angle.

$$\begin{pmatrix} (\underline{B}_u \times \underline{B}_d)_0 \\ (\underline{B}_u \times \underline{B}_d)_1 \\ \vdots \end{pmatrix} \cdot \begin{pmatrix} Nx \\ Ny \\ Nz \end{pmatrix} = 0$$

The number of constraints available for our shock normal determinations is quite variable. Furthermore, the quality of the data itself varies. If a shock is encountered in a quiet solar wind background, then "good" upstream and downstream

values can be measured. However under disturbed solar wind conditions, the measured "upstream" and "downstream" values may, in fact, not correspond to the appropriate instantaneous values. Thus, it is highly desirable to have an independent check of the accuracy of the obtained solutions. We can do this two ways in our inversion process. First, we can calculate the eigenvalues and eigenvectors of the 3 x 3 real symmetric matrix which is inverted in our solution. These correspond to three directions in space which are determined to an accuracy which is measured by the size of the associated eigenvalues. In analogy to finding the error in determining a minimum variance direction we let the minimum eigenvalue be a measure of the background noise level of the inversion method. Then the error in the minimum eigenvector direction, $\delta\phi$, in the plane perpendicular to the maximum eigenvector is given by:

$$\delta\phi = \sin^{-1} (\lambda_3/\lambda_2)^{1/2}$$

If the normal $\underline{N}$ makes an angle α to the direction of the maximum eigenvector then the error in the direction of $\underline{N}$ due to the error in the eigenvector directions along the eigenvector associated with the maximum eigenvalue λ_1 is:

$$\delta\beta_1 = \cos^{-1} (\cos^2\alpha + (1 - \lambda_3/\lambda_2)^{1/2} \sin^2\alpha)$$

The error in the plane orthogonal to the intermediate eigenvector is similar but smaller.

$$\delta\phi_2 = \cos^{-1} (\cos^2\gamma + (1 - \lambda_3/\lambda_1)^{1/2} \sin^2\gamma)$$

where γ is the angle between the normal and the eigenvector associated with the intermediate eigenvalue. As a final error estimate, $\delta\phi$, we have summed these two errors and list them in Table 1 together with the normals, shock speed and constraints used in the solutions.

As a second method of evaluating our normals we have compared the orientation of the vector constraints that we have used to determine the direction of the normal. The constraints, except for the separation vector constraints, should all be perpendicular to the normal. We have calculated the average deviation of the "normal" constraints from being strictly orthogonal and list those as $\delta\theta$ in Table 1. We note that although this estimate has a very straight-forward physical basis it is not a perfect measure because all constraints could be exactly perpendicular to the normal and not constrain the orientation of the normal at all if the constraints were mutually parallel.

Table 1 contains the best fit normals and the associated shock velocity measured in the observer's frame, together with our two error estimates, the first, $\delta\beta$, being an error estimate for the orientation of the normal and the second, $\delta\theta$, being the average angular deviation of the constraints from 90°. Finally, the constraints used in the determinations are given. The numbers refer to the spacecraft: 1-ISEE-1; 2-ISEE-2; 3-ISEE-3; 7-Prognoz 7 and 8-IMP-8. The letter 'T' designates a separation vector and time delay constraint. The symbol 'ΔB' signifies a vector field jump constraint; BUV signifies the cross product of the upstream field direction and the change in plasma flow velocity across the shock; BDV signifies the cross product of the downstream field and the change in plasma flow velocity across the shock. Finally, UCD signifies the cross product between upstream and downstream magnetic fields.

Table 1. Best Fit Normals

Day	N(GSE)	V km/s	$\delta\beta$	$\delta\theta$	Constraints
78 230	(-.747, -.433, .505)	422	2.4°	1.3°	T_{21}, T_{23}, T_{28}, ΔB_1, ΔB_3, ΔB_8, UV_1, DV_1, UV_3, DV_3
78 254	(-.895, -.134, .425)	436	8.6°	6.5°	T_{23}, T_{28}, ΔB_1, ΔB_3, ΔB_8, UV_1, DV_1, UV_3, DV_3
78 263	(-.943, -.278, -.182)	334	0.3°	10.1°	T_{21}, T_{23}, ΔB_1, ΔB_3, UV_1, DV_1, UV_3, DV_3
78 268	(-.768, -.633, -.092)	811	5.3°	-----	T_{23}, ΔB_3, UCD_3
78 271	(-.934, -.332, .135)	672	1.3°	3.1°	T_{21}, T_{23}, ΔB_1, ΔB_3, UV_1, DV_1, UV_3, DV_3
78 290	(-.860, -.374, .347)	395	0.3°	0.9°	T_{21}, T_{23}, ΔB_1, ΔB_3, UV_1, DV_1, UV_3, DV_3
78 302	(-.893, .054, .447)	424	4.1°	1.0°	T_{23}, T_{28}, ΔB_1, ΔB_3, ΔB_8, UV_1, DV_1, UV_3, DV_3
78 312	(-.882, -.193, .492)	447	3.8°	4.4°	T_{23}, ΔB_2, ΔB_3, UCD_2, UCD_3, UV_3, DV_3
78 316	(-.963, .095, -.253)	606	9.5°	6.6°	T_{13}, ΔB_1, ΔB_3, UCD_1, UV_1, DV_1
78 359	(-.802, -.488, .344)	432	3.3°	6.0°	T_{21}, T_{23}, T_{27}, ΔB_1, ΔB_3, UV_1, DV_1, UV_3, DV_3
79 243	(-.625, .288, -.725)	402	6.4°	9.6°	T_{21}, T_{23}, T_{28}, ΔB_1, ΔB_3, ΔB_8, UV_1, DV_1, UV_3, DV_3
79 315	(-.897, .368, .244)	466	11.1°	7.7°	T_{13}, ΔB_1, ΔB_3, UCD_1, UCD_3, UV_1, DV_1, UV_3, DV_3
79 322	(-.816, .568, -.103)	504	2.9°	4.4°	T_{21}, T_{23}, ΔB_1, ΔB_3, UV_1, DV_1, UV_3, DV_3
79 324	(-.445, -.688, .573)	282	14.1°	1.0°	T_{23}, ΔB_1, ΔB_3, UCD_1, UCD_3, UV_1, DV_1
79 333	(-.773, -.286, .567)	286	3.3°	3.1°	T_{21}, T_{23}, ΔB_1, ΔB_3, UV_1, DV_1, UV_3, DV_3
79 334	(-.978, -.047, -.201)	404	2.2°	3.0°	T_{21}, T_{23}, ΔB_1, ΔB_3, UV_1, DV_1, UV_3, DV_3

Legend

Spacecraft: 1, 2, 3, 7, 8 refer to ISEE 1, 2, 3, Prognoz 7 and IMP 8, respectively.

Constraints: T - Time delay and separation vector

ΔB - Change in magnetic field across shock

UCD - Vector cross product of upstream and downstream magnetic field

UV - Vector cross product of upstream magnetic field and velocity change

DV - Vector cross product of downstream magnetic field and velocity change

It is interesting to note which constraints were statistically the most accurate. The median deviation of the field jump from its expected orthogonality was only 2°, and 90% of the jumps were within 23° of being perpendicular to our fitted normal. The plasma jump constraints, BUV and BDV, were almost as good. The median errors were 7° and 6°, respectively, with 90% of the deviations less than 25° for both constraints. The UCD or magnetic coplanarity constraint did not do as well as the others. Its median error was 21° with 90% of the errors being 46° or less. The problem with this technique lies in the need to calculate a cross product of nearly parallel vectors in a noisy environment. It should be used only when the magnetic field is relatively quiet and the shock moderately strong, with a reasonably large angle between the upstream and downstream field directions. Otherwise it should not be used or else given little weight in the overall solution.

We emphasize that the shock normal we obtain is an average shock normal and that the instantaneous shock normal may and probably does differ from the average value. However, this "real" deviation will not alter the relative ranking of the various constraints. The change in field across the shock was most often in the expected direction and the two field-velocity jump constraints were only slightly worse. We note that if there were large deviations of the instantaneous shock normal from its average value we would not expect the median deviation of the field jump constraint from its expected 90° value to be as low as 2°.

Testing the Normals

Before proceeding to use these determined shock normals we will use the redundancy inherent in these data to test the normal. First we can check our estimate of shock speed using the continuity equation (cf. Abraham-Shrauner and Yun, 1976).

$$V_{sh} = (\rho_2 \underline{V}_2 - \rho_1 \underline{V}_1) \cdot \underline{N}/(\rho_2 - \rho_1)$$

where ρ_1 and ρ_2 are the upstream and downstream solar wind densities, $\underline{V}_1$ and $\underline{V}_2$ the corresponding solar wind velocities and $\underline{N}$ is our best fit shock normal. This computation has been performed for ISEE-1 and -3 for each of our shocks whenever there was a complete plasma scan both upstream and downstream of the shock. Table 2 shows the comparison of these speeds with the best fit speed. Only the shock of 9/25/78 has significantly different speeds. Reference to Table 1 shows that this is the shock with the least number of constraints used in the best fit normal determination. Five constraints appear to be the minimum necessary to be assured of a moderately accurate normal.

Another test we can perform is to compare the Mach number of the shock calculated from the best fit shock speed and the magnetosonic velocity corresponding to the observed plasma conditions with the Mach number necessary to give the observed field jump. We list both these Mach numbers for the two spacecraft in Table 2. The last two columns give the angle between the upstream field and the best fit shock normal for the two spacecraft.

The Mach numbers necessary to give the observed field jumps according to the Rankine-Hugoniot equations, RH1 and RH3, are always greater than 1, by definition. However, because of the imprecision of our measurements of the shock velocity, the solar wind velocity and the plasma density, the magnetosonic velocity that we

Table 2. Shock Parameters

		Shock Velocity			Magnetic Mach Numbers				θ_{Bn}	
Date	Day	Best Fit	Cont. 1	Cont. 3	BF1	BF3	RH1	RH3	1	3
8/18/78	230	422km/s	454km/s	431km/s	1.4	1.6	1.6	1.5	73°	78°
9/11/78	254	436	410	409	0.9	1.2	1.3	1.2	32	36
9/20/78	263	334	313	338	1.4	1.6	1.2	1.1	75	76
9/25/78	268	811	453	-	4.9	-	3.0	2.0	60	57
9/28/78	271	672	713	717	0.9	0.9	1.5	1.5	57	55
10/17/78	290	395	419	408	1.0	1.7	1.4	1.4	63	76
10/29/78	302	424	432	421	0.7	1.3	1.4	1.4	69	61
11/8/78	312	447	-	532	-	1.5	1.7	1.6	43	41
11/12/78	316	606	570	-	2.4	-	2.4	2.2	42	40
12/25/78	359	432	414	427	2.2	2.3	1.6	1.7	80	87
8/31/79	243	402	372	392	1.5	1.1	1.4	1.3	40	75
11/11/79	315	466	436	451	2.8	2.4	2.7	1.3	57	67
11/18/79	322	504	474	531	1.7	1.4	1.5	1.7	76	82
11/20/79	324	282	290	-	1.3	-	1.3	1.3	48	39
11/29/79	333	286	290	274	2.0	2.3	2.7	2.0	66	62
11/30/79	334	404	465	417	2.6	2.8	2.5	2.5	89	87

calculate is sometimes greater than the shock speed relative to the upstream plasma. Most often the difference between the two techniques is rather small. However, on 9/25/78 the difference is large. This is also the shock for which we found large differences with shock speed calculation and which had the fewest constraints. Because of these uncertainties, we will not use this shock in the analysis which follows. Further, to characterize the Mach number of the shocks we will use the "Rankine-Hugoniot" Mach numbers. The only exception to this will be the shock of 11/11/79 for which the Rankine-Hugoniot value from the ISEE-3 data differs significantly from the other three values. For this shock we will use the best fit value of 2.7.

Precursor Waves

Visual inspection of the interplanetary shock data reveals two upstream wave types. Furthest upstream from the shocks there is often irregular turbulence, whose frequency spectrum is featureless. Closer to the shock, but not observed as often, a nearly monochromatic wave, which we call a precursor wave, grows in amplitude and terminates at the shock. It does not extend downstream, in contrast to the irregular turbulence which is usually seen both upstream and downstream. It is important to distinguish these two wave types because they have very diff-

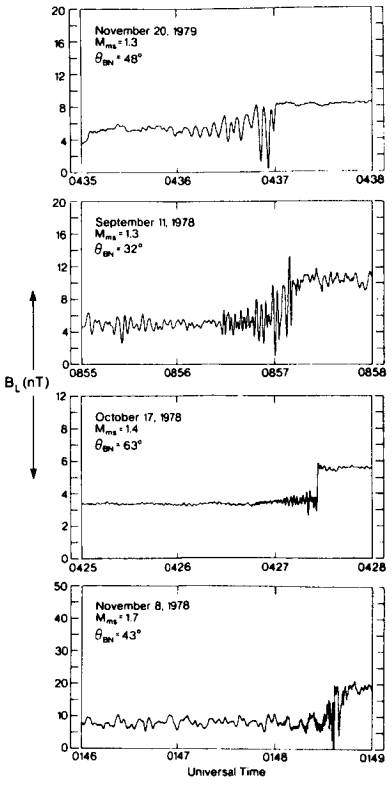

Figure 1. Whistler precursors for four interplanetary shocks as observed by ISEE-2. The component of the magnetic field shown is along the projection of the interplanetary magnetic field on the shock plane and contains the jump in the magnetic field across the shock.

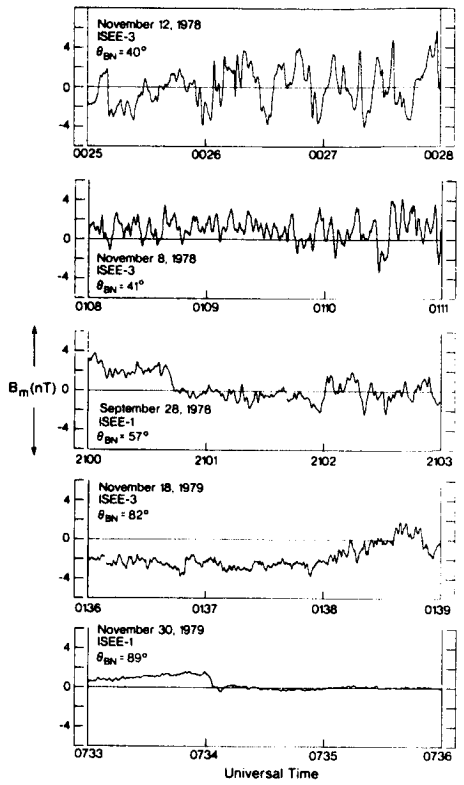

Figure 3. Turbulence seen upstream of five interplanetary shocks. The component shown is perpendicular to the upstream magnetic field and the shock normal.

erent properties. Figure 1 shows examples of the precursor waves for four shocks in the direction perpendicular to the projection of the upstream field on the shock plane. We have identified nine examples of such waves in our shock dataset. These events and their properties are listed in Table 3.

Power spectra were calculated over the duration of the precursor wave in shock normal coordinates (L, M, N) in which N is in the direction of the best fit normal and L is in the shock plane along the direction of the upstream magnetic field. A well defined spectral peak was found for each precursor. The frequency of this peak was calculated by multiplying the frequency by the power of each estimate of the power contributing to the peak, summing, and dividing by the power in the peak. These frequencies are listed in Table 3. The direction of the wave normal, the angle between the wave normal and the magnetic field direction, θ_{Bk}, the percent polarization and the eccentricity were calculated according to the method of Means (1972) and are also listed in this Table. For the ISEE-3 shock

on October 29, 1978 we used minimum variance analysis to get the wave normal because the data contained too many gaps for our usual wave analysis techniques to work. A glance at the wave normals reveals that the M components are small. Thus these waves are principally propagating in the plane defined by the shock normal and the upstream magnetic field. The waves generally propagate at a small angle to the magnetic field. The wave normal on September 28, 1978 made the largest angle to the field, almost 45°. This was also the briefest precursor, lasting only a few seconds. The percent polarization for all these waves is large, greater than 90% for every event and usually over 95%. The polarization for the precursors is very nearly circular and right-handed in every case but one, the August 18, 1978 event on ISEE-3. We believe that this apparent left-hand polarization is not real but that the wave is actually right-handed and oscillating at 3.74 Hz. The 3 Hz Nyquist frequency of ISEE-3 then aliases the signal to 2.26 Hz and reverses the polarity. The wave spectrum for ISEE-3 November 12, 1978 reveals two peaks both of which have precursor-like properties, i.e., small θ_{Bk}, large percent polarization and right-handed nearly circular polarization. It is not obvious why two waves are present for this case. We note that since these are forward propagating shocks, not reverse shocks like planetary bow shocks, we do not expect

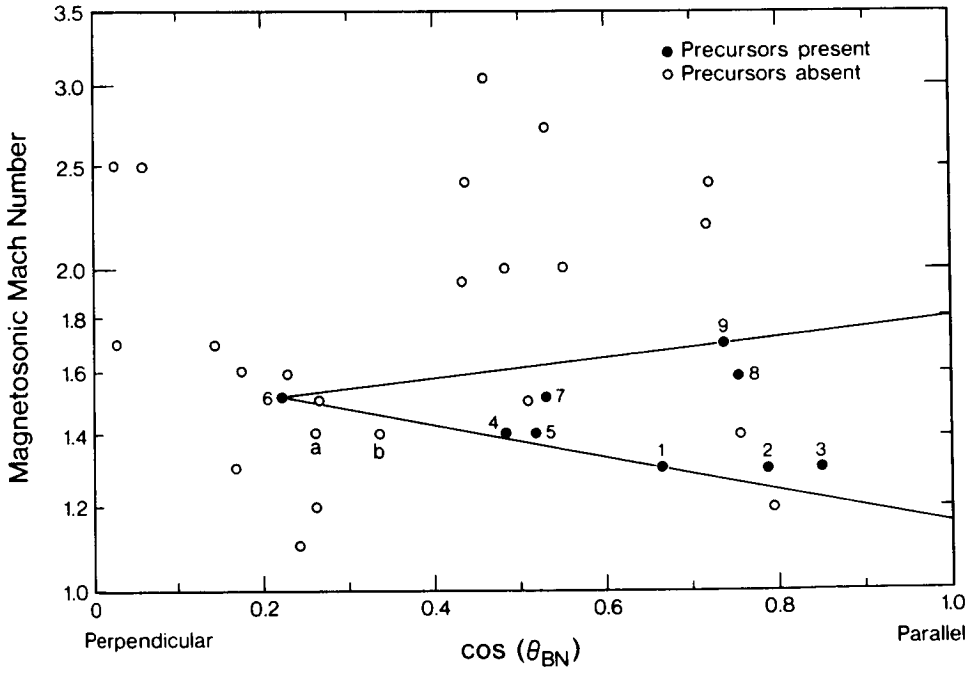

Figure 2. The location of the interplanetary shocks examined in the Mach number - cos θ_{Bn} plane. Solid circles are used to denote those shocks which had whistler precursors. The wedge encloses the region in which precursors were observed.

Doppler shifted polarization reversals. Hence the right-handed polarization identifies these as whistler mode waves.

A glance at Table 3 also reveals that these precursors are present only for shocks with M<1.7. Figure 2 shows the location of these events in the Mach number - $\cos(\theta_{Bn})$ plane. A wedge with its vertex at M = 1.5 and cos θ_{Bn} = .22 and its feet at M = 1.16 and 1.8 on the cos θ_{Bn} = 1.0 axis contains all the events. However, there are three shocks within this wedge without precursors. The first near point 6 is from ISEE-2 on November 18, 1979. No precursor waves were seen at ISEE-3 either on this day but none would be expected to be observed because the shock at ISEE-3 was stronger, M = 1.7, and more perpendicular. Perhaps the reason for no precursors at ISEE-2 is that we have incorrectly calculated the Mach number for the ISEE-2 shock. However, there is a simpler explanation. Table 3 reveals that the frequency of the wave at point 6, (ISEE-3 on 8/18/78), is observed to be at least 2.26 Hz and is probably 3.74 Hz. This is well above the ISEE-2 Nyquist frequency on November 18, 1979 of 2.0 Hz. Since the ISEE-2 magnetometer is strongly filtered above the Nyquist frequency before the signal is sampled, no aliased signal is telemetered by the spacecraft.

A second exception occurs near point 7. The exceptional point is from ISEE-1 on September 28, 1978 and point 7 is from ISEE-3 on this same day. Table 3 indicates that the (brief) precursor wave seen at ISEE-3 oscillated at 2.53 Hz. This again was well above the 2 Hz Nyquist frequency of ISEE-1 on September 28, 1978. The final exception is near point 2. This point corresponds to ISEE-2 observations on August 31, 1979. The nearby observations, points 1, 2 and 3, have frequencies well below the Nyquist frequency of ISEE-2. We note that ISEE-3 did not observe precursor waves but we would not have expected to observe them because the shock was very nearly perpendicular at ISEE-3 (θ_{Bn} = 80°). The only unusual condition in the solar wind on this day was that the upstream electron and ion temperatures were about equal. However, it is not obvious to us how this condition would affect the precursor waves.

It is obvious from Table 3 and our discussion above that the cause of the top leg of the wedge through points 6 and 9 is the disappearance of the precursor waves as they become undetectable above the passband of our instruments. We have no means of determining from these data how high in Mach number or frequency these waves extend.

The reason for the lower leg is not as obvious. The point below point 2 that has no precursors is, in fact, very unshock-like in the magnetic field. There is merely a very slow rise in field strength and rotation lasting 35 seconds. Perhaps this represents one cycle of a very long wavelength whistler wave. Points a and b do show some upstream wave activity. Point a corresponds to the ISEE-2 shock on October 29, 1978. The waves at ISEE-2 have properties very similar to the precursors discussed above. They propagate nearly along the magnetic field and they are highly polarized. However, they occur at a frequency an order of magnitude less than were observed on ISEE-3 for this same event. On the other hand, the waves corresponding to point b at ISEE-3 on October 17, 1978 are similar in frequency to those seen at ISEE-2 for this same event (point 4). However, these waves are propagating at a large angle to the field, are less well polarized, are elliptical rather than circular and are left-handed. Moreover they are weak and do not grow as the shock approaches. The frequency also is suspiciously close to the spin frequency of the spacecraft. The other three low Mach number cases at

M = 1.3, 1.2 and 1.1 correspond to ISEE-3 on August 31, 1979, ISEE-2 on September 20, 1978 and ISEE-3 on September 20, 1978. The first two cases are well defined sharp shocks with no precursors but have many data gaps upstream including one right at the shock crossing. The absence of precursor waves at the lowest Mach numbers appears to be a real phenomenon. Its explanation is not obvious.

Upstream Turbulence

In addition to the precursor waves which exist in the shock ramp and for a short distance upstream, irregular waves with rather featureless spectra are seen upstream of some interplanetary shocks. Figure 3 shows samples of these waves for a variety of angles between the upstream magnetic field and the shock normal. Figure 4 shows power spectra for these waves. The magnetic component shown is the M component, i.e., the direction in the plane of the shock perpendicular to the upstream field. As discussed in the previous section the precursor waves which we are able to observe are a low Mach number phenomenon. At higher Mach numbers the precursor waves occur at higher frequencies eventually rising above our pass band. To avoid mixing the two wave types we will use the simple expedient of studying the upstream turbulence only at Mach numbers above 1.5.

Table 4 shows the properties of the upstream turbulence for the one minute just prior to shock passage for all the interplanetary shocks in our study which had Mach numbers greater than 1.5 and were not contaminated with ions backstreaming from the terrestrial bow shock. We have also eliminated any intervals for which we did not have a full minute of upstream measurements and those for which an obvious tangential discontinuity occurred during the analysis interval. The frequency interval 0.03 to 0.3 Hz was chosen for analysis. There is little power in these waves above 0.3 Hz and 30 seconds is as low a period one could safely analyze utilizing a minute's worth of data. We have used the analysis of Born and Wolf (Rankin and Kurtz, 1970) as it is more appropriate for the study of linearly polarized signals such as these waves tend to be.

As for the precursors, the wave normals in L, M, N, coordinates show that the waves are mainly propagating in a plane defined by the magnetic field and the shock normal. Further, the waves are propagating nearly parallel to the magnetic field. For the two exceptions to this rule, ISEE-3 on December 25, 1978 and ISEE -2 on November 30, 1979, it may be argued that since the shocks are very nearly perpendicular and the waves very small that the direction of propagation is not well determined. The percent polarization is much less than for the precursors ranging from 26 to 73%. The waves are polarized about equally left and right-handed and are at times very nearly linearly polarized. The maximum eccentricity observed was 0.76. The waves are almost entirely transverse fluctuations, as shown by the last column of Table 4 which gives the ratio of compressional power to transverse power. Except for two nearly perpendicular shocks which have almost no transverse power upstream, this ratio is less than 10%. This is consistent with the observed direction of propagation of the waves which is nearly parallel to the field and in contrast to waves upstream of the bow shock.

The amplitudes of these waves are strongly correlated with θ_{Bn}, the angle between the upstream magnetic field and the shock normal. Figure 5 shows the logarithm of the amplitude of the waves as a function of the cos θ_{Bn}. The straight line is the best fit straight line omitting the two low points on November 29, 1979. It has a correlation coefficient of 0.935. If we include the two low

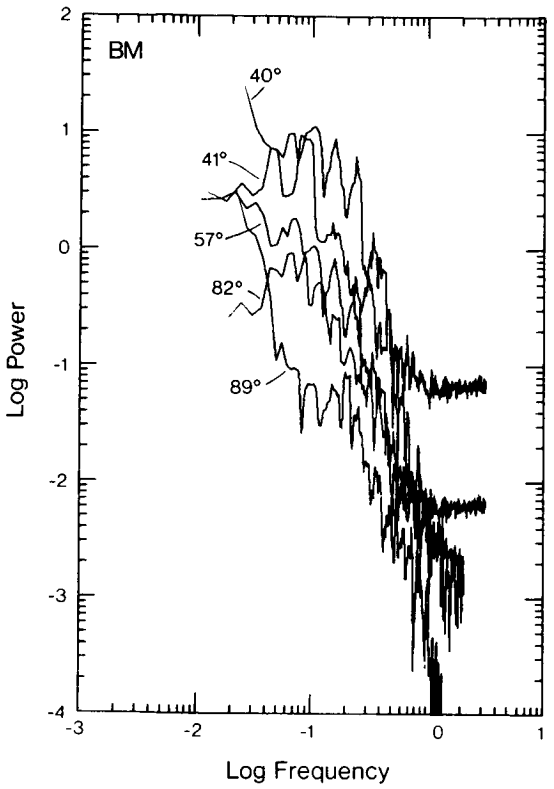

Figure 4. Power spectra of the waves shown in Figure 3.

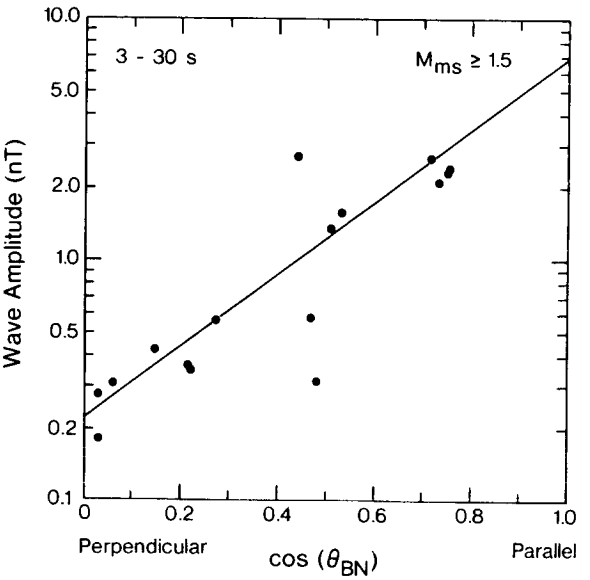

Figure 5. The logarithm of the wave amplitude of upstream turbulence as a function of the cosine of the angle between the interplanetary field and the shock normal. The amplitude is the square root of the trace of the spectral matrix integrated over the frequency band from 0.03 to 0.3 Hz.

Table 4. Properties of Upstream Turbulence

Day	Spacecraft	Mach No.	θ_{Bn}	Amplitude	Wave Normal	θ_{Bk}	%P	ε	% Comp.
8/10/78	3	1.5	78^{o}	0.36nT	(.953, -.021, -.185)	4.0^{o}	51.7%	-0.12	.009
8/18/78	2	1.6	73	0.37	(.974, .032, -.226)	4.0	66.3	-0.76	.034
9/28/78	1	1.5	57	1.37	(.872, -.059, .487)	3.4	29.3	0.56	.034
11/8/78	3	1.6	41	2.33	(.638, .150, -.756)	9.1	60.4	0.70	.039
11/8/78	2	1.7	43	2.12	(.670, .079, -.738)	3.7	25.9	0.36	.069
11/12/78	3	2.2	40	2.71	(-.519, -.084, -.850)	13.7	56.5	-0.26	.031
12/25/78	3	1.6	87	0.28	(-.629, -.081, -.773)	52.6	61.4	0.21	.239
11/11/79	3	2.4	67	2.70	(-.843, -.151, -.517)	10.6	58.5	-0.56	.029
11/11/79	2	2.7	57	1.57	(-.690, -.181, -.701)	16.8	73.0	0.68	.051
11/18/79	3	1.7	82	0.44	(.935, -.010, -.355)	14.3	68.2	0.01	.013
11/18/79	2	1.5	76	0.56	(.937, .300, .181)	18.3	48.4	0.15	.071
11/29/79	3	2.0	62	0.31	(-.943, -.212, -.257)	18.3	33.0	-0.21	.061
11/29/79	2	2.7	66	0.58	(-.838, .027, -.546)	6.3	32.6	-0.01	.025
11/30/79	3	2.5	87	0.31	(-.788, .364, -.497)	35.3	72.6	-0.02	.071
11/30/79	2	2.5	89	0.18	(-.864, .500, .066)	58.6	72.4	0.39	.230

November 29 points the correlation drops to 0.838. However, on November 29 the upstream magnetic field strength is only 2.5 nT, less than half its usual magnitude. Since we expect that these waves grow through resonance with the upstream ions we expect that the ion gyro frequency orders these waves. Then the spectral power of the waves would occur on this day at a much lower frequency and our one minute analysis interval is not long enough to determine the proper wave power. It seems clear that the wave amplitudes are controlled by θ_{Bn}. We note that we have used here a one minute average of the upstream field just upstream of the shock to define θ_{Bn}. In actuality, the waves observed were generated at an earlier time when the IMF may have had a different direction. Furthermore, the presence of discontinuities in the solar wind can add power to the wave analysis even though they have no association with the shock.

Discussions and Conclusions

The results of our investigations of waves upstream from interplanetary shocks indicate that, while their successful study is difficult, they can be profitably examined if data from both magnetometers and plasma instruments are available. The most important step in this process is determining an accurate normal. The mixed mode technique for a single spacecraft appears to be quite accurate in general. When an accurate normal is available, the shock speed can be determined quite accurately from the continuity equation. However, to guarantee an accurate normal determination one should use data from multiple spacecraft and overdetermine the solution. This allows calculation of probable error and the time delay between spacecraft gives the velocity, independent of the plasma measurements.

In sorting out the plethora of phenomena associated with interplanetary shocks, it is important to realize that there are two different wave types in the upstream region with quite different wave properties. The precursor waves are an integral part of the shock structure at low Mach numbers at moderate and small angles of the IMF to the shock normal. These waves are right-handed and are obviously propagating in the direction of the shock motion, that is with the solar wind flow. Thus, while they are Doppler shifted, their polarization is not reversed. Hence, they must also be right-handed, i.e., whistler mode waves, in the plasma frame also. The whistler precursors are highly polarized and are very nearly circularly polarized.

At the lowest Mach numbers and for nearly perpendicular shocks, there seem to be few waves upstream of the shock. However, above a Mach number of 1.5 there are broadband irregular waves with low to moderate percent polarization, propagating generally at small angles to the field with almost linear polarization. The amplitude of these waves is strongly correlated with the direction of the IMF relative to the shock normal. These waves seem to be those predicted by Lee (1983).

Much analysis is yet to be done with both the precursor waves and the upstream turbulence. For example, we have not investigated what controls the wavelength or direction of propagation and hence the apparent frequency of the precursor waves. Nor have we examined their amplitude and duration. Similarly, we must examine the full spectrum of the upstream turbulence, not just the arbitrary 3-30 second band, and the size of the region of occurrence of these waves upstream of interplanetary shocks.

Acknowledgments. This work was supported by the National Aeronautics and Space Administration at UCLA under research contract NAS5-27752, at the Jet Propulsion Laboratory as one phase of research carried out under NAS7-100, and at Los Alamos under the auspices of the U.S. Department of Energy with support from NASA under contract S-50864A.

References

Abraham-Shauner, B. and S.H. Yun, Interplanetary shocks seen by Ames plasma probe on Pioneer 6 and 7, J. Geophys. Res., 81, 2097-2102, 1976.

Axford, W.I., Acceleration of cosmic rays by shock waves, in Proceedings of an International School and Workshop on Plasma Astrophysics held at Varenna, Como, Italy, from 27 August to 7 September 1981 (ESA SP-161), pp. 425-449, ESTEC, Noordwijk, Holland, 1981.

Bame, S.J., J.R. Asbridge, H.E. Felthauser, J.P. Gore, G. Paschmann, P. Hemmerich, K. Lehmann and H. Rosenbauer, ISEE-1 and ISEE-2 fast plasma experiment and the ISEE-1 solar wind experiment, IEEE Trans. Geoscience Electronics, GE-16, 216, 1978a.

Bame, S.J., J.R. Asbridge, H.E. Felthauser, J.P. Gore, H.L. Hawk and J. Chavez, ISEE-C solar wind plasma experiment, IEEE Trans. Geosci. Electronics, GE-16, 160-162, 1978b.

Frandsen, A.M.A., B.V. Connor, J. Van Amersfoort and E.J. Smith, The ISEE-C vector helium magnetometer, IEEE Trans. Geoscience Electronics, GE-16, 195-198, 1978.

Gosling, J.T., S.J. Bame, W.C. Feldman, G. Paschmann, N. Sckopke and C.T. Russell, Suprathermal ions upstream from interplanetary shocks, J. Geophys. Res., 88, in press, 1983.

Hoppe, M.M. and C.T. Russell, On the nature of ULF waves upstream of planetary bow shocks, in Advances in Space Research, 1, 327-332, 1981.

Kennel, C.F., F.L. Scarf, F.V. Coroniti and E.J. Smith, Nonlocal plasma turbulence associated with interplanetary shocks, J. Geophys. Res., 87, 17-34, 1982.

Lee, M.A., Coupled hydromagnetic wave excitation and ion acceleration at interplanetary travelling shocks, J. Geophys. Res., submitted, 1983.

Means, J.D., Use of the three-dimensional covariance matrix in analyzing the polarization properties of plane waves, J. Geophys. Res., 77, 5551, 1972.

Morfill, G. and M. Scholer, Solar cosmic ray diffusion coefficient behind interplanetary shock waves, in Contributed Papers to the Study of Travelling Interplanetary Phenomena/1977, (edited by M.A. Shea, D.F. Smart and S.T. Wu), pp. 231-241, 1977.

Rankin, D. and R. Kurtz, Statistical study of micropulsation polarizations, J. Geophys. Res., 75, 5444-5458, 1970.

Russell, C.T., The ISEE-1 and -2 fluxgate magnetometers, IEEE Trans. Geoscience Electronics, GE-16, 239-242, 1978.

Russell, C.T. and M.M. Hoppe, Upstream waves and particles, Space Sci. Rev., in press, 1983.

Russell, C.T., M.M. Mellott, E.J. Smith and J.H. King, Multiple spacecraft observations of interplanetary shocks: Four spacecraft determination of shock normals, J. Geophys. Res., submitted, 1983a.

Russell, C.T., J.T. Gosling, R. Zwickl and E.J. Smith, Multiple spacecraft observations of interplanetary shocks: ISEE 3-D plasma measurements, J. Geophys. Res., submitted, 1983b.

Tsurutani, B.T., E.J. Smith and D.E. Jones, Waves observed upstream of interplanetary shocks, J. Geophys. Res., submitted, 1983.